

Stability of alkali-metal oxides as a function of pressure: Theoretical calculations

Ž. Čančarević, J. C. Schön, and M. Jansen

Max-Planck-Institut für Festkörperforschung, Heisenbergstrasse 1, D-70569 Stuttgart, Germany

(Received 20 September 2005; revised manuscript received 14 March 2006; published 27 June 2006)

We investigate the regions of thermodynamic stability of possible modifications of the alkali oxides M_2O as a function of pressure and type of alkali metal ($M=Li, Na, K, Rb, Cs$). The results are in good agreement with experiment at standard pressure, and we find that at elevated pressures, all systems should exhibit a transition from the experimentally observed modifications (CaF₂- and CdCl₂-type) to one or more high-pressure modifications exhibiting structures belonging to the extended cotunnite family, e.g., the high-pressure (hp)-BaF₂-, the PbCl₂-, the γ -US₂-, or the Θ -Ni₂Si-type. Metastable modifications that would be stable at sufficiently large negative pressures exhibit the CaCl₂- or the CdCl₂-structure type.

DOI: [10.1103/PhysRevB.73.224114](https://doi.org/10.1103/PhysRevB.73.224114)

PACS number(s): 61.50.Ah, 61.50.Ks, 61.66.Fn, 71.15.Nc

I. INTRODUCTION

In recent years, experiments at very high pressures exceeding 10 GPa have become more common,^{1,2} leading to an enormous increase in the number of new high-pressure phases discovered in various chemical systems. However, in spite of highly improved experimental techniques, the *in situ* measurements of the structure of these compounds are still far from trivial, and in many instances, the only reliable information obtained is the cell constants of the modification under investigation. Thus, it would be very helpful in the identification of newly generated phases, if one could supplement the experimental results by theoretical investigations on the same system. As a consequence, in a number of chemical systems predictions of high-pressure phases have been made^{3–17} by computing $E(V)$ curves for several possible structure candidates that had usually been suggested by chemical intuition or drawn from a database of existing structures, such as the inorganic crystal structure database (ICSD).^{18,19}

But not only has the high-pressure range received increased attention, even more fascinating is the observation that new experimental techniques lead to metastable compounds that would be thermodynamically stable at negative pressures. An instance of a synthesis at effective negative pressures is realized by the growth of crystalline compounds in an amorphous matrix of the same atomic composition that had been deposited at very low temperatures (liquid nitrogen or liquid helium temperature) using atom beams.^{20,21} In many cases,^{20–23} the modification formed when employing this method has proven to be a low-density phase that would be the thermodynamically preferred one only at high temperatures or negative pressures, reminiscent of Ostwald's rule.²⁴ This can be explained by taking into account that the amorphous matrix usually exhibits an even lower density than the crystalline nuclei belonging to the many possible modifications. Thus, the forces experienced by the nuclei at the matrix-crystal interface result in an effective negative pressure, favoring the formation of low-density phases.²³

This poses a challenge to the theoretician, since one can no longer expect that all relevant structure candidates at high positive and negative pressures are also local minima of the potential energy, i.e., of the enthalpy at zero pressure. In-

stead, it is necessary to study the enthalpy surface for many different pressures, in order to determine as many candidates as possible for such extreme conditions. The procedure is completely analogous to structure prediction for solids at low (zero) pressure via the determination of local minima of the potential energy of the system.^{25–29} In earlier work,^{13,30,31} we have shown for several binary nitrides, sulfides, and oxides, how one can identify such structures and predict the transition pressures among them.

Clearly, it would be of interest to know to what extent these landscapes differ within a family of chemically related systems. Here, the well-known pressure homologue rule³² for families of compounds, as applied to transition pressures, must be mentioned in the first place. According to this rule, the pressure-induced transitions between two modifications within a family of compounds take place at decreasing pressure for increasing size of the cations for fixed choice of the anion. Our investigations point to the fact that one should view the traditional pressure homologue rule as “one-half” of the full rule, which is based on the analysis of regions of stability of families of compounds along the pressure axis.³⁰

Specifically, we are going to investigate the alkali oxides, since there exist a number of experimental observations^{33–41} and theoretical calculations,^{42–47} which can be employed to validate the computations presented here. We note that most of the experimental and theoretical work found in the literature is focused on Li₂O since this compound has been considered as a potential candidate for blanket breeding material in nuclear reactors.⁴⁴ There appears to be a great variety in high-pressure structure types in the alkali metal oxides, many of which belong to the extended cotunnite family.⁴⁸ In agreement with experiment, for Cs₂O and the other oxides, the CdCl₂- and the CaF₂-structure type, respectively, are found to be stable at standard pressure.

II. METHODS

A. General approach

Quite generally, the structure candidates that should be capable of existence, at least at low temperatures, correspond to local minima of the enthalpy hypersurface ($H=E_{\text{pot}}+pV$) of the chemical system under investigation. Experience has

shown that many metastable modifications of a chemical compound can be capable of existence at various temperatures and pressures, and that it is not necessarily the thermodynamically stable one that is found as the outcome or as an intermediary product of a particular synthesis route or natural chemical process. Thus, the goal of the landscape exploration is the determination of as many of the low-lying local minima as possible. Both identifying the energetically favored candidate for a given set of thermodynamic parameters and finding the candidates that represent metastable modifications requires the use of a global optimization method, where, in general, we permit free variation of atom positions, cell parameters, ionic charges, and composition.

Since such global searches for local minima involve many millions of energy evaluations for atomic configurations, one usually cannot perform the energy calculation using *ab initio* methods or very refined but computationally expensive empirical potentials. Thus, it is necessary to split the search procedure into several modules. First, one performs global optimizations using a simple but robust empirical potential to describe the interaction energy between the different atoms and ions. This results in a large set of several thousand configurations that correspond to local minima on the empirical energy or enthalpy landscape. Next, these configurations are sifted to remove duplicates and to sort them into structure families. The remaining set of distinct structure candidates is then locally optimized on the *ab initio* level, and the $E(V)$ curves for all structure candidates are computed. This allows us to decide which of the possible modifications is thermodynamically stable and which are close in energy but metastable, at a given pressure at low temperatures. Finally, extending this analysis to higher temperatures requires the computation of the free energy and/or enthalpy in the harmonic and quasi-harmonic approximation. For further details regarding our general approach to the determination of structure candidates we refer to the literature.²⁵

B. Modeling the landscape

In order to perform global searches for local minima on the energy and/or enthalpy landscapes of a chemical system that exhibits strongly ionic character, we model the chemical system as an assembly of spherical atoms and ions that interact via a simple empirical two-body interaction potential, $V_{ij}(r_{ij})$, consisting of a Coulomb and a Lennard-Jones-term that depend only on the atom-atom distance r_{ij} . This allows fast calculations of the energy, $E_{\text{pot}} = \sum_{i < j} V_{ij}(r_{ij})$, of a given configuration,

$$V_{ij}(r_{ij}) = \frac{q_i q_j}{r_{ij}} \exp(-\mu r_{ij}) + \epsilon_{ij} \left[\left(\frac{\sigma_{ij}}{r_{ij}} \right)^{12} - \left(\frac{\sigma_{ij}}{r_{ij}} \right)^6 \right]. \quad (1)$$

The parameters entering the empirical potential are the sum of the ionic radii multiplied by a scaling factor r_s , $\sigma_{ij} = r_s(i)r_{\text{ion}}(i) + r_s(j)r_{\text{ion}}(j)$, the parameters ϵ_{ij} , and the convergence parameter μ . We note that if higher precision is needed, we compute the electrostatic energy during the global optimization stage by employing a computationally more expensive Ewald summation (formally corresponding to $\mu = 0$), as proposed by de Leeuw *et al.*,⁴⁹ instead of a conver-

gence parameter μ . But, at this stage we are mostly interested in calculational speed and in the possible structures, and not so much in their precise energies or cell parameters, which are computed in the second stage on the *ab initio* level during local optimizations.

Clearly, we cannot expect the ranking of the candidates by energy to always agree with the one found after the local optimization on the *ab initio* level. However, at the global stage of the exploration, the goal is the identification of as many reasonable structure candidates as possible. Thus, we repeat our search for ranges of values of the parameters r_s (typically, =1.0–1.2), ϵ_{ij} (typically, =0.3–0.5) and μ (typically =0.05–0.15), since this allows us to access a much larger range of potential structure candidates. Furthermore, repeating the sets of optimization runs for different values of the parameters allows us to judge the robustness of the structure candidates.⁵⁰ We note that this approach also allows us to take into account that for a number of atoms their ionic radii can vary as function of coordination sphere.^{51,52}

Since we are interested in crystalline compounds, we always introduce periodic boundary conditions and employ up to 40 atoms per simulation cell. Although our general move class also involves changes of composition, we have found it to be more efficient to keep the composition fixed and to repeat the runs for different compositions, and for each composition for different numbers of formula units per simulation cell.

In the work presented here, we have employed $Z=2, 3$, and 4 formula units of the respective compounds, per simulation cell. Furthermore, we have kept the composition ($M:X=2:1$) and the charges ($q_{\text{cation}}=+1$, $q_{\text{anion}}=-2$) fixed, since preliminary work had shown⁵⁰ that all the relevant low-energy structures were found in that part of the energy landscape, where both the alkali metals and the oxygen atoms are ionized. The ionic radii employed during the optimization of the alkali metal oxides were:⁵³ $r_{\text{ion}}(\text{Li}^+) = 0.78 \text{ \AA}$, $r_{\text{ion}}(\text{Na}^+) = 0.98 \text{ \AA}$, $r_{\text{ion}}(\text{K}^+) = 1.33 \text{ \AA}$, $r_{\text{ion}}(\text{Rb}^+) = 1.49 \text{ \AA}$, $r_{\text{ion}}(\text{Cs}^+) = 1.65 \text{ \AA}$, and $r_{\text{ion}}(\text{O}^{2-}) = 1.40 \text{ \AA}$. We note that due to our general choice of interaction potential, the appearance of O_2^- and O_2^{2-} units is very unlikely, since the formation of covalent oxygen-oxygen bonds is not energetically favored.⁵⁴

The calculations were repeated for a number of pressures, starting with a pressure of 1.6 atmosphere and increasing in steps by a factor of 10 up to 16 Mbar, and similarly for negative pressures up to -1.6 Mbar. Each choice of pressure corresponds to a different enthalpy landscape given by $H = E_{\text{pot}} + pV$, of course. The reason for this choice of pressures is that, due to the functional form of the core-repulsion potential ($V \propto r^{-12}$), we expect the changes in the landscape between subsequent high values of pressure to occur at considerably larger absolute pressure differences than at low-pressure values. Because of the rather widely spaced set of pressure values and the limitations of the interaction potential, the calculation of the transition pressure is not possible at this stage, but we can expect to gain a good overview over the structure candidates as function of pressure. The possible phase transitions between these candidates will then be determined at the *ab initio* stage of the procedure.

C. Optimization procedures

The global optimizations in this work were performed employing the stochastic simulated annealing algorithm,^{55,56} which is based on random walks on the energy landscapes. Each step from configuration x_i to a neighbor x_{i+1} is accepted according to the Metropolis criterion,⁵⁷ with a temperature schedule $T_n = T_0 \gamma^n$ ($\gamma = 0.95 - 0.995$). The move class consisted of atom movement (80% of all the moves), atom exchange (5% of all the moves), and random variations of the cell parameters (15% of all the moves), keeping the ionic charges fixed. Since the structure candidates were found using a simple empirical potential as a cost function, we are faced with two problems.

First, we note that the structure candidates will usually not exhibit any obvious symmetries (they are given in space group $P1$, due to the unrestricted optimization procedure). To deal with this issue, we use several algorithms SFND,⁵⁸ RGS,⁵⁹ and CMPZ⁶⁰ that have been implemented in the program KPLOTT.⁶¹ SFND,⁵⁸ short for SYMMETRIEFINDER (=symmetry finder), identifies all symmetries of a periodic structure, where only the atomic coordinates are given as input. RGS,⁵⁹ short for RAUMGRUPPENSUCHER (=space group searcher), determines for a given set of symmetries the space group of the structure. Finally, CMPZ,⁶⁰ short for COMPARE ZELLEN (=compare cells), performs a comparison of a given pair of periodic structures and determines whether these structures are the same within some given set of tolerances. With the help of these algorithms and appropriate script programs, LOAD and FILTER,⁶² we can determine the symmetries and space groups of all minimum configurations of the enthalpy landscapes we have identified, eliminate duplicates, and group these structures into families. For more details on the working of these algorithms, refer to the references given.

Second, since we had to use empirical parameters for the ionic radii and Lennard-Jones-interaction strengths, the nearest-neighbor distances among the atoms are not necessarily in agreement with those one would observe in experiment. Both the size of the unit cell and the relative atom positions might differ somewhat from the experimental values, making a comparison between predicted and subsequently synthesized compounds difficult.

Thus, when we rank the candidates by energy, employing the *ab initio* program CRYSTAL2003,⁶³ we still need to perform a local optimization of the cell parameters and atom positions. In order to deal with the problem in an efficient way, we have developed a heuristic algorithm HARTREE,^{30,62} which performs the local optimization in an automated fashion. These local optimizations take place via a nested sequence of line searches, where the outer cycles deal with the optimization of the cell parameters and the inner ones with the optimization of the atom positions. If necessary (e.g., when going to perform phonon calculations), the final line-search optimization of the atom positions is followed by a gradient-based energy minimization. For more details, refer to the references.

During these local optimizations, we usually restricted the variation of the cell parameters and atom positions, such that the space group symmetry, which had been determined dur-

ing the idealization stage, was preserved. In order to gain an estimate of the validity of the *ab initio* calculations, we have performed both Hartree-Fock and density functional theory (DFT) [functional: B3LYP (Refs. 64 and 65)] calculations for all structures and systems. In addition to the optimized cell parameters, these calculations yield the bulk modulus B_0 by fitting the calculated data points to the Murnaghan equation,⁶⁶

$$E(V) = \frac{VB_0}{B'_0} \left[\frac{(V_0/V)^{B'_0}}{B'_0 - 1} + 1 \right] - C, \quad (2)$$

where the four fit parameters B_0 and B'_0 are the bulk modulus and its derivative, V_0 the equilibrium volume, and C the zero of the energy scale, respectively. By calculating the enthalpies $H_i = E_i(V) + pV = E_i(V) - (\partial E / \partial V)V$ for the various structure candidates i , one can determine the transition pressures between different modifications i and j by setting the enthalpies equal, $H_i = H_j$.⁶⁷

D. Choice of basis sets

The choice of basis sets is a crucial step of the calculation, since we have to balance two conflicting issues: accuracy and computational cost,⁶⁸ while taking the minimum basis set requirements into account. Basis sets for Li, Na, K, and O were taken from the literature, where they had been proposed for Li_2O , Na_2O , and K_2O .^{42,43} For Rb and Cs in Rb_2O and Cs_2O , we employed basis sets that had been optimized in the context of our study on alkali metal sulfides.³⁰

III. RESULTS

A. Results of the global search

An overview over the different structure candidates found in the five alkali oxide systems as function of pressure is given in Fig. 1. For each pressure range and alkali oxide, the different structure types with space groups other than $P1$ or $P-1$ that had been observed are listed and are represented by a symbol. The number of times a given type has appeared is indicated by the number inside the symbol. Not counting structures with space group $P1$ or $P-1$, about 60 different structure types were observed to constitute local minima on the various enthalpy landscapes. About half of these candidate structures could be identified with experimentally known structure types, using the automated structure comparison script FILTER,⁶⁹ which employs the CMPZ algorithm.⁶⁰ A list of the new structure types is given in the Appendix (see Tables IV–XIII).

We note that for some of the alkali oxides, extended families of structure types, such as the cotunnite,⁴⁸ the fluorite, or the rutile structure family, are represented not only with one but with several local minima in the same chemical system. For instance, for Li_2O , we find as important local minimum structures in the cotunnite family not only the PbCl_2 -type structure, but also the high-pressure (hp)- BaF_2 -type structure, the γ - US_2 -type structure, and the Θ - Ni_2Si -type structure.⁷⁰ This is clearly not a side-effect of the use of the empirical potentials, since in nearly all cases these structure

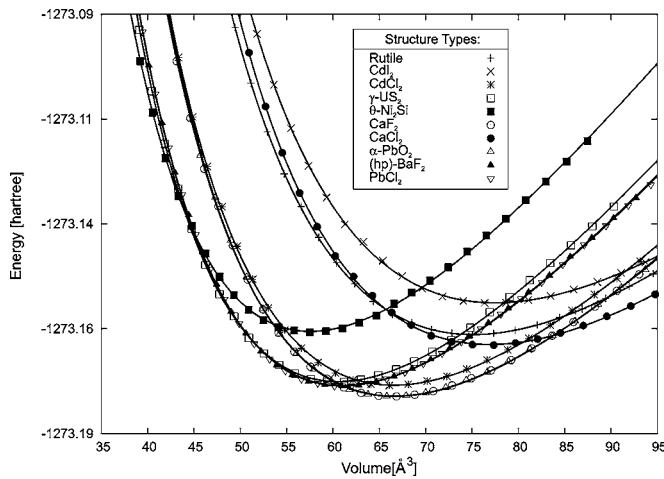


FIG. 4. Selected $E(V)$ curves for K_2O calculated using an all-electron basis set via the Hartree-Fock method.

tion methods, since at negative pressures well-ordered low-density crystalline structures always compete with a plethora of slab-, rod-, or clusterlike structures that often exhibit very low enthalpies.³¹

B. *Ab initio* results

About 60 structures belonging to local minima observed on the enthalpy landscapes of the oxides M_2O together with the additional structures mentioned above were chosen for the local optimizations on the *ab initio* level. For the remaining candidates, it was checked whether their *ab initio* energies were sufficiently low to warrant a local optimization. If so, they were included in the local optimization step of the analysis. For the quantum mechanical calculations, we have employed both the Hartree-Fock approximation (HF) and a DFT functional [B3LYP⁶⁵]. Figures 2–6 show the $E(V)$ curves for the five oxide systems, the alkali metal oxides M_2O ($M=Li, Na, K, Rb, Cs$), calculated in the HF approximation. For comparison, Fig. 7 depicts the $E(V)$ curves using

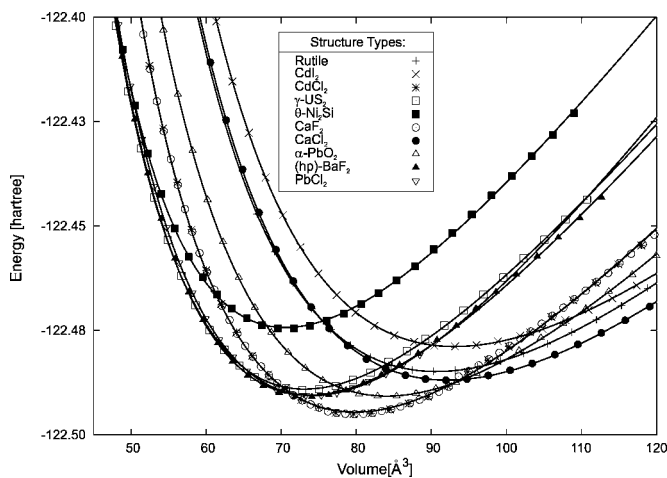


FIG. 5. Selected $E(V)$ curves for Rb_2O calculated using a pseudopotential basis set for Rb and all-electron basis set for O via the Hartree-Fock method.

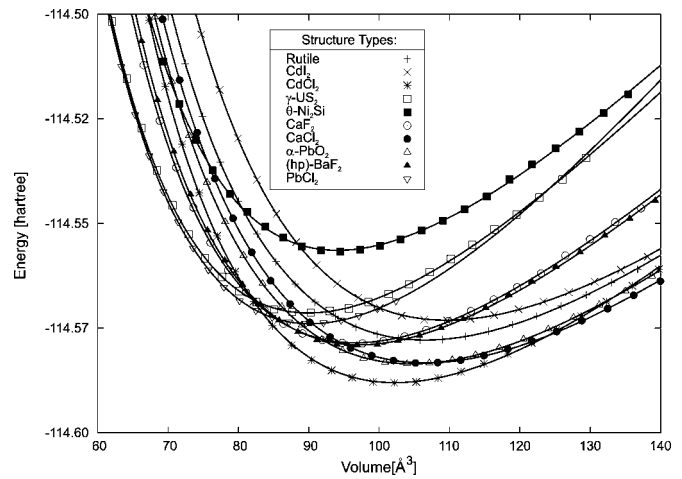


FIG. 6. Selected $E(V)$ curves for Cs_2O calculated using a pseudopotential basis set for Cs and all-electron basis set for O via the Hartree-Fock method.

the DFT method for K_2O . The two sets of curves are rather similar, with the most noticeable difference being the larger slope in the HF-curves for large volumes. [The DFT-based curves for the other oxides, and additional plots focusing on high- and low-pressure ranges of the systems are given in the supplementary material.⁷² Only one-third—about 20 different structure types—of the $E(V)$ curves per system are shown, in order to avoid overcrowding of the pictures.]

We only show the curves for the most important structure types for each specific system, in particular, the $CdCl_2$ -, CaF_2 -, $PbCl_2$ -, rutile-, $CaCl_2$ -, α - PbO_2 -, γ - US_2 -, (hp)- BaF_2 -, and Θ - Ni_2Si -type, in order to avoid cluttering the pictures. We note that some structures such as rutile and $CaCl_2$, PdF_2 , and CaF_2 , or $PbCl_2$ and (hp)- BaF_2 ,⁷³ are very closely related and properly belong to the same basin of the empirical energy landscape of M_2O . In all systems except Cs_2O , the local *ab initio* optimization of the candidates with the $PbCl_2$ - and (hp)- BaF_2 -structure type has resulted in essentially the same optimized structure for much of the volume range, based on the standard tolerances for the CMPZ algorithm.

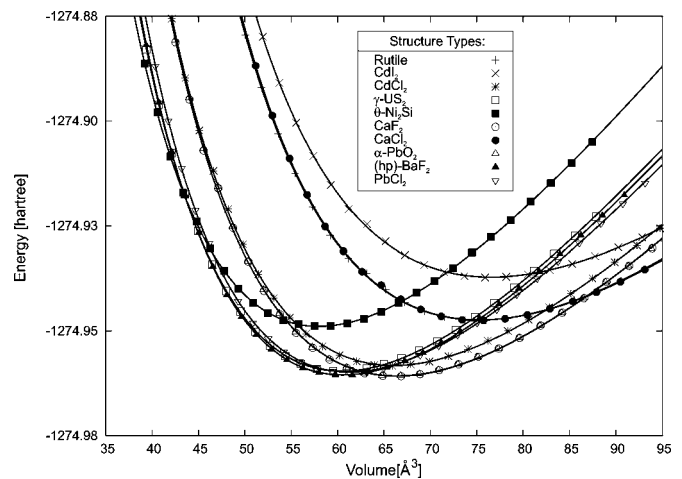


FIG. 7. Selected $E(V)$ curves for K_2O calculated using an all-electron basis set via the DFT-B3LYP method.

TABLE I. Volume V (in \AA^3), energies (in hartree), and bulk moduli B (in GPa) of the structure candidates at zero pressure, calculated using different *ab initio* techniques. Note that the experimental volumes refer to the volume at transition pressure, while the calculated ones refer to zero pressure.

Chemical system	Hamiltonian	Structure candidates									Observation
		CdCl ₂	CaCl ₂	CaF ₂	(hp)-BaF ₂	PbCl ₂	α -PbO ₂	γ -US ₂	Θ -Ni ₂ Si		
Li ₂ O	HF	73.515	54.685	94.757	90.628	89.630	106.792	66.029	44.813	$V_{CaF_2}=97.97-98.55^a$	
		-89.9578	-89.9524	-89.9627	-89.9504	-98.9501	-89.9530	-89.9472	-89.9379		
		100.766	89.324	102.554	107.127	107.722	91.310	109.580	108.157		$B_{CaF_2}=89^b$
	DFT	74.178	54.555	95.803	91.033	90.648	106.887	66.929	45.413		
		-90.4350	-90.4294	-90.4394	-90.4293	-90.4288	-90.4302	-90.4260	-90.4181		
		96.802	88.109	97.912	104.202	104.232	90.045	105.470	104.658		
Na ₂ O	HF	127.006	93.041	161.891	150.232	152.307	161.822	111.440	70.232	$V_{CaF_2}=170.95^c$	
		-398.6839	-398.6796	-398.6898	-398.6838	-398.6836	-398.6896	-398.6824	-398.6698		
		59.090	55.148	62.180	66.085	65.089	62.084	66.415	68.207		
	DFT	127.097	93.117	163.989	153.815	155.028	164.067	114.048	72.643		
		-399.8567	-399.8522	-399.8615	-399.8580	-399.8579	-399.8604	-399.8565	-399.8449		
		56.789	54.092	58.631	64.614	63.855	58.370	61.819	60.623		
K ₂ O	HF	199.309	153.568	266.180	243.954	244.104	266.030	181.345	115.037	$V_{CaF_2}=225.87-266.59^d$	
		-1273.1785	-1273.1686	-1273.1811	-1273.1788	-1273.1787	-1273.1812	-1273.1777	-1273.1658		
		40.159	33.230	40.748	45.257	45.089	40.100	45.972	48.938		
	DFT	197.676	150.420	265.089	241.970	244.901	265.028	181.013	115.733		
		-1274.9633	-1274.9523	-1274.9658	-1274.9656	-1274.9650	-1274.9658	-1274.9647	-1274.9541		
		39.310	33.396	38.692	45.092	44.287	38.703	45.165	47.017		
Rb ₂ O	HF	239.182	184.025	318.864	294.334	278.412	335.593	219.316	141.140	$V_{CaF_2}=306.45-308.23^e$	
		-122.4997	-122.4919	-122.4998	-122.4957	-122.4725	-122.4957	-122.4942	-122.4795		
		35.794	28.945	35.842	39.703	52.84	32.993	40.134	43.489		
	DFT	235.731	180.059	314.122	290.575	277.498	328.915	216.551	139.755		
		-123.4091	-123.3995	-123.4090	-123.4068	-123.3856	-123.4049	-123.4054	-123.3926		
		36.252	29.266	35.857	40.282	44.052	33.486	41.165	44.333		
Cs ₂ O	HF	306.010	212.984	386.569	389.315	360.217	417.930	270.163	188.440	$V_{CaCl_2}=297.89^f$	
		-114.5880	-114.5833	-114.5785	-114.5794	-114.5740	-114.5835	-114.5715	-114.5565		
		28.333	24.714	29.582	30.521	38.974	25.332	34.404	33.548		
	DFT	293.234	206.106	371.562	361.652	347.829	397.233	263.162	181.108		
		-115.4997	-115.4929	-115.4896	-115.4895	-115.4860	-115.4934	-115.4856	-115.4694		
		30.074	25.469	30.196	33.070	34.073	26.785	34.646	33.625		

^aSee Refs. 33 and 34.

^bSee Ref. 45.

^cSee Ref. 33.

^dSee Refs. 33, 35, and 99.

^eSee Refs. 36 and 37.

^fSee Ref. 38.

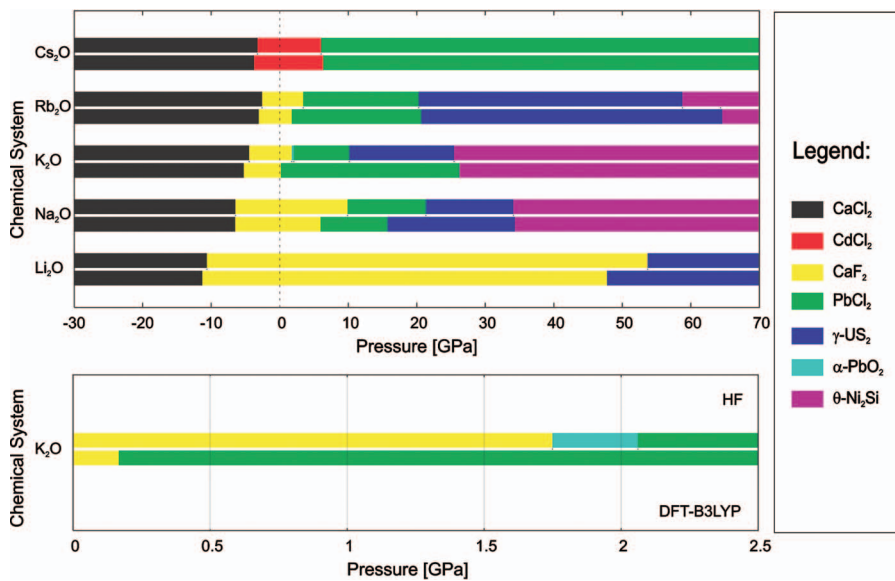


FIG. 8. (Color) Low temperature modifications of alkali metal oxides M_2O as function of pressure ($M=Li, Na, K, Rb,$ and Cs). As discussed in the text, usually several possible modifications exist for a given pressure that are only separated by a very small amount of enthalpy [cf. the $E(V)$ curves for the M_2O systems]. Only the modifications with the lowest enthalpy are depicted. Upper line: HF. Lower line: DFT-B3LYP. For K_2O we also show more details of the pressure range between 0 and 2.5 GPa.

From the $E(V)$ curves, we can calculate the bulk moduli of the various modifications. Their values, as well as the computed and observed cell volumes, are found in Table I for some of the most relevant structure types in each of the alkali metal oxides, i.e., the $CdCl_2$ -type, the $CaCl_2$ -type, the CaF_2 -type, the (hp)- BaF_2 -type, the α - PbO_2 -type, the γ - US_2 -type, the Θ - Ni_2Si -type, and the $PbCl_2$ -type. We show the results for both the HF and the DFT calculation.

C. Stability regions as function of pressure

From the $E(V)$ curves, we can determine the thermodynamically stable phases as a function of pressure. These are depicted in Fig. 8, in the form of one-dimensional phase diagrams. For each system, the transition pressures between the different modifications computed using the HF and DFT methods, respectively, are plotted. At standard pressure (≈ 0 GPa), the experimentally observed CaF_2 -type modification is stable, except for Cs_2O , where the $CdCl_2$ -type is stable, in agreement with experiment. The $CaCl_2$ -type modification is the thermodynamically stable one in all systems for sufficiently large negative pressures (see Table II).

For elevated positive pressures, several modifications belonging to the cotunnite family, the (hp)- BaF_2 -type, the $PbCl_2$ -type, the γ - US_2 -type, and the Θ - Ni_2Si -type, and as an intermediary the α - PbO_2 -type, are in very close competition. This group is followed, at very high pressures, by the Li_2O -VII-type, the Rb_2O -III-type, and the Ni_2In -type (not shown in Fig. 8). The transition pressures for the five oxides are given in Table II. With the exception of Cs_2O , there appears to exist a general sequence $CaCl_2 \rightarrow CaF_2 \rightarrow [(hp)\text{-}BaF_2, PbCl_2, \alpha\text{-}PbO_2] \rightarrow \gamma\text{-}US_2 \rightarrow \Theta\text{-}Ni_2Si$, where not all members are actually present in each system.

The $CdCl_2$ -type appears to be metastable in all systems (except for Cs_2O , where it is stable at standard pressure) and in close competition with the CaF_2 -type. The stability of the $CdCl_2$ -type increases with cation size along the group from Li_2O to Rb_2O , until it becomes completely stable for Cs_2O . Furthermore, in the case of Rb_2O , the energy difference be-

tween the $CdCl_2$ -type and the CaF_2 -type is within the accuracy of the calculation.

When comparing the diagrams for the different oxides, we see that for $M=Li, \dots, Rb$, the transition from CaF_2 to the first high-pressure phase approximately follows a rule analogous to the pressure-homologue rule, i.e., the larger the cation, the lower the transition pressure. However, the corresponding transitions in the negative pressure regime show the “opposite” trend: the larger the cation, the higher (i.e., less negative) the pressure. It appears that the quantity that changes monotonically with increasing cation size is actually the stability range of the phase(s) in the interior of the phase diagram, e.g., the range of stability of the CaF_2 -type modification decreases with increasing cation size, until the CaF_2 -type becomes completely metastable for Cs_2O .

IV. DISCUSSION

The data in Tables I and III, and in the tables in the Appendix show that there is a satisfactory agreement between the computed and observed values. Considering the cell parameters of the modifications that are stable at standard pressure, we see that the difference lies below 2%. Concerning the bulk moduli, there appear to exist only data for Li_2O : $B_{exp}^{Li} = 89$ GPa (Ref. 40) vs $B_{th}^{Li} = 98\text{--}102$ GPa. Finally, there are recent indications⁴¹ that there might occur a phase transition in Li_2O at about 45–50 GPa, possibly to a cotunnite-type structure. These observations would be in agreement with our calculations, which show a transition in that pressure range to one of the two cotunnite-type modifications, $PbCl_2$ -type or γ - US_2 -type, that possess nearly the same enthalpy at these pressures, within the limits of the computational accuracy. A comparison between our calculations and those presented in the literature for Li_2O , Na_2O , and K_2O shows good agreement.

To a certain extent, the difference between theory and experiment can be connected to systematic shortcomings of the *ab initio* methods: HF and DFT typically overestimate and underestimate cell parameters, respectively. The differ-

TABLE II. Transition pressures for alkali metal oxides.

Chemical system	Hamiltonian	Transition	Pressure (GPa)
Li ₂ O	HF	CaCl ₂ → CaF ₂	10.63
		CaF ₂ → γ-US ₂	53.70
		γ-US ₂ → Li ₂ O-Type-VII	219.16
	DFT	CaCl ₂ → CaF ₂	-11.30
		CaF ₂ → γ-US ₂	47.76
		γ-US ₂ → Li ₂ O-Type-VII	199.85
Na ₂ O	HF	CaCl ₂ → CaF ₂	-6.48
		CaF ₂ → (hp)-BaF ₂	9.91
		(hp)-BaF ₂ → γ-US ₂	21.32
		γ-US ₂ → θ-Ni ₂ Si	34.11
	DFT	CaCl ₂ → CaF ₂	-6.50
		CaF ₂ → (hp)-BaF ₂	5.96
K ₂ O	HF	(hp)-BaF ₂ → γ-US ₂	15.73
		γ-US ₂ → θ-Ni ₂ Si	34.33
		CaCl ₂ → CaF ₂	-4.47
		CaF ₂ → α-PbO ₂	1.75
	DFT	α-PbO ₂ → (hp)-BaF ₂	2.06
		(hp)-BaF ₂ → γ-US ₂	10.16
Rb ₂ O	HF	γ-US ₂ → θ-Ni ₂ Si	25.45
		CaCl ₂ → CaF ₂	-5.36
		CaF ₂ → (hp)-BaF ₂	0.17
		(hp)-BaF ₂ → θ-Ni ₂ Si	26.23
	DFT	CaCl ₂ → CaF ₂	-2.58
		CaF ₂ → (hp)-BaF ₂	3.42
Cs ₂ O	HF	(hp)-BaF ₂ → γ-US ₂	20.26
		γ-US ₂ → θ-Ni ₂ Si	58.77
		θ-Ni ₂ Si → Rb ₂ O-Type-III	64.32
		CaCl ₂ → CaF ₂	-3.06
	DFT	CaCl ₂ → CaF ₂	1.75
		CaF ₂ → (hp)-BaF ₂	20.64
CS ₂ O	HF	(hp)-BaF ₂ → γ-US ₂	64.60
		γ-US ₂ → θ-Ni ₂ Si	73.68
	DFT	θ-Ni ₂ Si → Rb ₂ O-Type-III	73.68
		CaCl ₂ → CdCl ₂	-3.25
		CdCl ₂ → PbCl ₂	6.04
		CaCl ₂ → CdCl ₂	-3.74
		CdCl ₂ → PbCl ₂	6.36

ence between HF and DFT is not strongly visible in the calculations presented here, since the B3LYP functional contains a larger exchange contribution than the standard LDA functional, and thus tends to interpolate between the DFT-LDA results and the HF results. A similar trend in secondary quantities such as transition pressures ($p_{\text{DFT}} < p_{\text{HF}}$) and bulk moduli ($B_{\text{DFT}} < B_{\text{HF}}$) is observed in most cases. However, for these secondary quantities, it is not clear whether there exist systematic general deviations of theoretical calculations from experimental values.

The results presented here appear to follow the general “trends” as far as the DFT calculations are concerned, but for the smaller cations, the HF approximation also slightly underestimates the experimental cell constants. However, this deviation is within the general accuracy of the *ab initio* calculations. Quite generally, one needs to always keep in mind that in addition to the systematic errors, there remain small but poorly controlled (essentially random) sources of error in the calculations. These are connected to both the inherent deficiencies of the basic approximations (HF and the various DFT functionals), and, within these methods, to the choice (and size) of basis sets and/or pseudopotentials. In addition, relativistic effects can play a role for the larger cations, in particular, Cs.⁷⁴ Thus, there still can exist sizeable error bars on the computed quantities, even after one has taken the systematic trends into account. For instance, our experience³⁰ shows that, without fine-tuning (which is not possible when predicting structures), the predicted transition pressures are only accurate to within several gigapascal (GPa), and the bulk moduli within about 30% of the experimental value.

Going beyond these considerations concerning the precise values of, e.g., the transition pressures, we turn to the question of the general stability of the various phases as function of pressure. First, we note that for most pressure ranges there exists a tight competition between two or even more modifications, as can be clearly seen in Figs. 2–7, and the $E(V)$ curves in the supplementary material. Thus, within the limits of accuracy of the *ab initio* programs currently available, one cannot make a final decision, which among these modifications is the thermodynamically stable one at low temperatures. Furthermore, one needs to be aware of the possibility that an actual experimental synthesis route following a par-

TABLE III. Calculated and experimental lattice parameters for the minimum structure type in the M_2O system ($M=\text{Li,Na,K,Rb,Cs}$).

System, Structure, Cell parameter(s)	Li ₂ O, CaF ₂ -type, a (Å)	Na ₂ O, CaF ₂ -type, a (Å)	K ₂ O, CaF ₂ -type, a (Å)	Rb ₂ O, CaF ₂ -type, a (Å)	Cs ₂ O, CdCl ₂ -type, a/c (Å)	
This work	HF	4.56	5.45	6.43	6.83	4.35/18.67
	DFT-B3LYP	4.58	5.47	6.42	6.80	4.23/18.89
Literature	Calculation (Refs.)	4.52–4.64 (41–43, 45, and 47)	5.39–5.66 (42, 43, 45, and 47)	6.17–6.47 (42, 43, and 47)		
	Experiments (Refs.)	4.61–4.63 (33, 34, 41, 100, and 101)	5.55 (33)	6.44 (33, 35, and 99)	6.74–6.76 (36 and 37)	4.26/18.99 (36, 38, and 39)

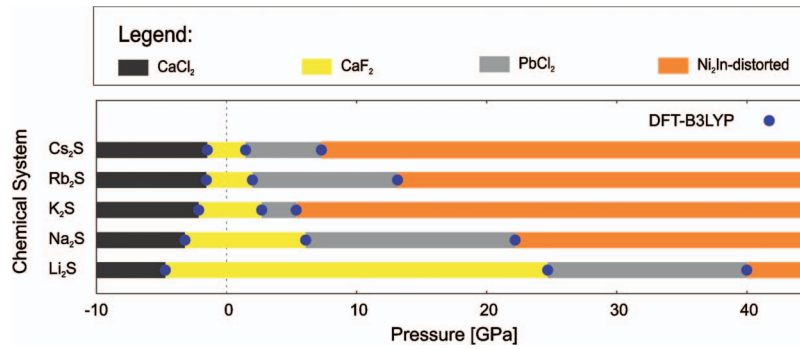


FIG. 9. (Color) Low temperature modifications of alkali metal sulfides M_2S as function of pressure ($M=Li, Na, K, Rb,$ and Cs) calculated using DFT-B3LYP. Concerning Cs_2S , the CaF_2 and the $PbCl_2$ structures are in close competition, with the Hartree-Fock results preferring the CaF_2 -type, and some DFT calculations the $PbCl_2$ -type, respectively. However, since it was not possible to calculate a sufficiently accurate estimate of the temperature dependence of the free enthalpy on the *ab initio* level, we cannot draw any final conclusion as to whether the $PbCl_2$ -type modification that is experimentally observed at room temperature is also going to be the thermodynamically stable one at zero temperature. For more details, see Ref. 30.

TABLE IV. Data for structure candidates for Li_2O after local optimizations on the *ab initio* level (Hartree-Fock).

Space group (no.) crystal system, type	Lattice constants a, b, c (Å); α, β, γ (°)	Atom (multip., Wyckoff lett.), rel. coord.				V_{\min} (Å ³) B (GPa)	E_{\min} (a.u.)
		atom	x	y	z		
$R-3m$ (166) <i>trigonal</i>	$a=3.18097$ $\alpha=\beta=\gamma=62.21145$	Li1(2c)	0.77459	0.77459	0.77459	23.884	-89.9529
Li_2O -type-I		O1(1a)	1/2	1/2	1/2	101.525	
$I4/mmm$ (139) <i>tetragonal</i>	$a=2.71045$ $c=5.84713$	Li1(4e)	0	0	0.34976	42.956	-89.9063
Li_2O -type-III	$\alpha=\beta=\gamma=90$	O1(2a)	0	0	0	113.995	
$Pmmn$ (59) <i>orthorhombic</i>	$a=2.89200$ $b=5.46531$ $c=2.68815$	Li1(4e)	1/4	0.91045	0.41042	42.488	-89.8737
Li_2O -type-IV	$\alpha=\beta=\gamma=90$	O1(2a)	1/4	1/4	0.06985		
$Cmc2_1$ (36) <i>orthorhombic</i>	$a=3.45063$ $b=5.26532$ $c=5.01866$	Li1(4a)	0	0.36803	0.92413	91.182	-89.9413
Li_2O -type-VI	$\alpha=\beta=\gamma=90$	Li2(4a)	0	0.91410	0.15924		
$P-3m1$ (164) <i>trigonal</i>	$a=3.42078$ $c=4.11232$	O1(4a)	0	0.72911	0.79968		
Li_2O -type-VII	$\alpha=\beta=90$	Li1(2d)	1/3	2/3	0.77189	41.674	-89.9157
$Pmna$ (62) <i>orthorhombic</i>	$a=3.97915$ $b=3.97915$ $c=5.61163$	Li2(1b)	0	0	1/2	114.632	
Li_2O -type-IX	$\alpha=\beta=90$	Li3(1a)	0	0	0		
$P432_12$ (96) <i>tetragonal</i>	$a=4.12923$ $c=5.00368$	O1(2d)	1/3	2/3	0.26822		
Li_2O -type-XI	$\alpha=\beta=\gamma=90$	Li1(4c)	0.19604	1/4	0.92823	88.852	-89.8854
Li_2O -type-XII	$a=2.83482$ $b=7.26264$ $c=4.15082$	Li2(4c)	0.02103	1/4	0.28765	110.493	
Li_2O -type-XII	$\alpha=\beta=\gamma=90$	O1(4c)	0.72980	1/4	0.89272		
$P432_12$ (96) <i>tetragonal</i>	$a=4.12923$ $c=5.00368$	Li1(8b)	0.37980	0.86214	0.84476	85.315	-89.7567
Li_2O -type-XI	$\alpha=\beta=\gamma=90$	O1(4a)	0.88668	0.88668	0		
$Cmcm$ (63) <i>orthorhombic</i>	$a=2.83482$ $b=7.26264$ $c=4.15082$	Li1(4c)	0	0.09706	1/4	85.458	-89.7770
Li_2O -type-XII	$\alpha=\beta=\gamma=90$	Li2(4b)	0	1/2	0		
Li_2O -type-XII	$\alpha=\beta=\gamma=90$	O1(4c)	0	0.81304	1/4		

TABLE V. Data for structure candidates for Li₂O after local optimizations on the *ab initio* level (DFT-B3LYP).

Space group (no.) crystal system, type	Lattice constants <i>a</i> , <i>b</i> , <i>c</i> (Å); <i>α</i> , <i>β</i> , <i>γ</i> (°)	Atom (multip., Wyckoff lett.), rel. coord.				<i>V</i> _{min} (Å ³) <i>B</i> (GPa)	<i>E</i> _{min} (a.u.)
		atom	<i>x</i>	<i>y</i>	<i>z</i>		
<i>R</i> −3 <i>m</i> (166) <i>trigonal</i>	<i>a</i> =3.19172 <i>α</i> = <i>β</i> = <i>γ</i> =62.21145	Li1(2c) O1(1a)	0.77459 1/2	0.77459 1/2	0.77459 1/2	24.127 97.223	−90.4302
Li ₂ O-type-I							
<i>I4</i> / <i>mmm</i> (139) <i>tetragonal</i>	<i>a</i> =2.72900 <i>c</i> =5.88713	Li1(4e) O1(2a)	0 0	0 0	0.34976 0	43.844 107.375	−90.3876
Li ₂ O-type-III	<i>α</i> = <i>β</i> = <i>γ</i> =90						
<i>Pmmn</i> (59) <i>orthorhombic</i>	<i>a</i> =2.91655 <i>b</i> =5.51171	Li1(4e) O1(2a)	1/4 1/4	0.91045 1/4	0.41042 0.06985	43.579 102.973	−90.3579
Li ₂ O-type-IV	<i>c</i> =2.71097 <i>α</i> = <i>β</i> = <i>γ</i> =90						
<i>Cmc</i> 2 ₁ (36) <i>orthorhombic</i>	<i>a</i> =3.46488 <i>b</i> =5.28707	Li1(4a) Li2(4a)	0 0	0.36803 0.91410	0.92413 0.15924	92.317 101.610	−90.4199
Li ₂ O-type-VI	<i>c</i> =5.03938 <i>α</i> = <i>β</i> = <i>γ</i> =90	O1(4a)	0	0.72911	0.79968		
<i>P</i> −3 <i>m</i> 1 (164) <i>trigonal</i>	<i>a</i> =3.44323 <i>c</i> =4.13930	Li1(2d) Li2(1b)	1/3 0	2/3 0	0.77189 1/2	42.500 111.202	−90.3978
Li ₂ O-type-VII	<i>α</i> = <i>β</i> =90	Li3(1a) O1(2d)	0 1/3	0 2/3	0 0.26822		
<i>Pmna</i> (62) <i>orthorhombic</i>	<i>a</i> =3.99617 <i>b</i> =3.99617	Li1(4c) Li2(4c)	0.19604 0.02103	1/4 1/4	0.92823 0.28765	89.998 110.082	−90.3698
Li ₂ O-type-IX	<i>c</i> =5.63564 <i>α</i> = <i>β</i> = <i>γ</i> =90	O1(4c)	0.72980	1/4	0.89272		
<i>P432</i> ₁ 2 (96) <i>tetragonal</i>	<i>a</i> =4.16697 <i>c</i> =5.04941	Li1(8b) O1(4a)	0.37980 0.88668	0.86214 0.88668	0.84476 0	87.676 104.972	−90.2514
Li ₂ O-type-XI	<i>α</i> = <i>β</i> = <i>γ</i> =90						
<i>Cmcm</i> (63) <i>orthorhombic</i>	<i>a</i> =2.84903 <i>b</i> =7.29905	Li1(4c) Li2(4b)	0 0	0.09706 1/2	1/4 0	86.750 110.370	−90.2710
Li ₂ O-type-XII	<i>c</i> =4.17163 <i>α</i> = <i>β</i> = <i>γ</i> =90	O1(4c)	0	0.81304	1/4		

ticular temperature and pressure schedule might result in one of the metastable compounds instead of the thermodynamically stable one. It would therefore be recommended to compare the result of a high-pressure synthesis also to all the close competitors and not only to (according to the calculations) the thermodynamically stable modification.

The importance of knowing not only the thermodynamically stable phase but also having information about its closest competitors touches on the final possible source of error, the use of a simple empirical potential for the energy calculation during the global landscape exploration, which might result in missing important structure candidates. Quite generally, there exist a large number of empirical potentials of ever increasing complexity that have been employed to model ionic compounds. These range from two-body potentials, such as the Buckingham-potential,⁷⁵ the Born-Huggins-Meyer-potential,⁷⁶ the simple robust potential we have been using or a refined version thereof with environment dependent radii,^{51,52} over dipole⁷⁷ and quadrupole⁷⁸ shell

models, to various kinds of breathing potentials^{5,79–91} of increasing levels of refinement. The latter ones are discussed more fully in several reviews.^{92–94} Examples include Gordon-Kim-type approaches [modified electron gas (MEG), potential induced breathing (PIB), variationally induced breathing (VIB), and self-consistent charge deformation model (SCAD)], and Slater-Koster-type tight-binding methods.

Although the more refined potentials typically allow us to compute at least some properties of a given material with relatively high accuracy, it is not clear whether their use during the global optimization would be worth the cost as long as we are only interested in identifying possible structure candidates in a chemical system. For one, such potentials tend to be much more complicated and computationally expensive than the simple potentials we usually employ. Second, the number of parameters involved typically increases with the complexity of the potential, which makes it very difficult to construct such a potential without detailed *a pri-*

TABLE VI. Data for structure candidates for Na₂O after local optimizations on the *ab initio* level (Hartree-Fock).

Space group (no.) crystal system, type	Lattice constants a, b, c (Å); α, β, γ (°)	Atom (multip., Wyckoff lett.), rel. coord.				V_{\min} (Å ³) B (GPa)	E_{\min} (a.u.)
		atom	x	y	z		
<i>C2/m</i> (12) <i>monoclinic</i> Na ₂ O-type-I	$a=7.52240$	Na1(4i)	0.70405	0	0.89028	222.150	-398.6562
	$b=3.27336$	Na2(4i)	0.84953	0	0.58376	65.816	
	$c=9.02894$	Na3(4i)	0.44251	0	0.78609		
	$\alpha=\gamma=90$	O1(4i)	0.84819	0	0.31732		
	$\beta=92.26520$	O2(2a)	0	0	0		
<i>Pmna</i> (62) <i>orthorhombic</i> Na ₂ O-type-II	$a=4.73795$	Na1(4c)	0.88884	1/4	0.49749	143.189	-398.5629
	$b=4.07211$	Na2(4c)	0.27215	1/4	0.69699	59.210	
	$c=7.42167$	O1(4c)	0.89420	1/4	0.13502		
	$\alpha=\beta=\gamma=90$						
<i>Pbcm</i> (57) <i>orthorhombic</i> Na ₂ O-type-III	$a=4.65918$	Na1(4c)	0.67884	1/4	0	146.880	-398.5349
	$b=6.60135$	Na2(4d)	0.35638	0.04895	1/4	53.433	
	$c=4.77552$	O1(4d)	0.14717	0.39860	1/4		
	$\alpha=\beta=\gamma=90$						
<i>P2₁</i> (4) <i>monoclinic</i> Na ₂ O-type-IV	$a=7.04106$	Na1(2a)	0.43963	0.00234	0.98755	150.305	-398.6791
	$b=5.83139$	Na2(2a)	0.09853	0.99460	0.41493	66.560	
	$c=3.66966$	Na3(2a)	0.16929	0.66894	0.93910		
	$\alpha=\gamma=90$	Na4(2a)	0.31079	0.33761	0.41755		
	$\beta=94.00860$	O1(2a)	0.13479	0.24399	0.90073		
		O2(2a)	0.36475	0.73845	0.45534		
<i>P2₁2₁2₁</i> (19) <i>orthorhombic</i> Na ₂ O-type-V	$a=4.95784$	Na1(4a)	0.77578	0.79876	0.67363	143.585	-398.6668
	$b=3.90358$	Na2(4a)	0.47381	0.79291	0.94558	68.464	
	$c=7.41913$	O1(4a)	0.23166	0.20597	0.14705		
	$\alpha=\beta=\gamma=90$						

TABLE VII. Data for structure candidates for Na₂O after local optimizations on the *ab initio* level (DFT-B3LYP).

Space group (no.) crystal system, type	Lattice constants a, b, c (Å); α, β, γ (°)	Atom (multip., Wyckoff lett.), rel. coord.				V_{\min} (Å ³) B (GPa)	E_{\min} (a.u.)
		atom	x	y	z		
<i>C2/m</i> (12) <i>monoclinic</i> Na ₂ O-type-I	$a=7.58860$	Na1(4i)	0.70405	0	0.89028	228.070	-399.8316
	$b=3.30221$	Na2(4i)	0.84953	0	0.58376	59.501	
	$c=9.10839$	Na3(4i)	0.44251	0	0.78609		
	$\alpha=\gamma=90$	O1(4i)	0.84819	0	0.31732		
	$\beta=92.26520$	O2(2a)	0	0	0		
<i>Pmna</i> (62) <i>orthorhombic</i> Na ₂ O-type-II	$a=4.83975$	Na1(4c)	0.88884	1/4	0.49749	152.620	-399.7521
	$b=4.15961$	Na2(4c)	0.27215	1/4	0.69699	48.662	
	$c=7.58114$	O1(4c)	0.89420	1/4	0.13502		
	$\alpha=\beta=\gamma=90$						
<i>Pbcm</i> (57) <i>orthorhombic</i> Na ₂ O-type-III	$a=4.76437$	Na1(4c)	0.67884	1/4	0	157.054	-399.7284
	$b=6.75038$	Na2(4d)	0.35638	0.04895	1/4	43.290	
	$c=4.88333$	O1(4d)	0.14717	0.39860	1/4		
	$\alpha=\beta=\gamma=90$						
<i>P2₁</i> (4) <i>monoclinic</i> Na ₂ O-type-IV	$a=7.08829$	Na1(2a)	0.43963	0.00234	0.98755	153.350	-399.8533
	$b=5.87051$	Na2(2a)	0.09853	0.99460	0.41493	62.524	
	$c=3.69428$	Na3(2a)	0.16929	0.66894	0.93910		
	$\alpha=\gamma=90$	Na4(2a)	0.31079	0.33761	0.41755		
	$\beta=94.00860$	O1(2a)	0.13479	0.24399	0.90073		
		O2(2a)	0.36475	0.73845	0.45534		
<i>P2₁2₁2₁</i> (19) <i>orthorhombic</i> Na ₂ O-type-V	$a=5.00643$	Na1(4a)	0.77578	0.79876	0.67363	147.849	-399.8418
	$b=3.94184$	Na2(4a)	0.47381	0.79291	0.94558	65.970	
	$c=7.49186$	O1(4a)	0.23166	0.20597	0.14705		
	$\alpha=\beta=\gamma=90$						

TABLE VIII. Data for structure candidates for K₂O after local optimizations on the *ab initio* level (Hartree-Fock).

Space group (no.) crystal system, type	Lattice constants a, b, c (Å); α, β, γ (°)	Atom (multip. Wyckoff lett.), rel. coord.				V_{\min} (Å ³) B (GPa)	E_{\min} (a.u.)
		atom	x	y	z		
C2 (5) <i>monoclinic</i> K ₂ O-type-I	$a=19.84731$	K1(4c)	0.07822	0.92669	0.52962	402.275	-1273.1747
	$b=4.44091$	K2(4c)	0.08240	0.43873	0.06776	39.724	
	$c=4.56827$	K3(4c)	0.23285	0.92288	0.76198		
	$\alpha=\gamma=90$	O1(2a)	0	0.95014	0		
Immm (71) <i>orthorhombic</i> K ₂ O-type-II	$\beta=92.46470$	O2(4c)	0.16011	0.41961	0.58447		-1273.1747
	$a=4.12478$	K1(4j)	1/2	0	0.72688	131.777	
	$b=4.66090$	O1(2a)	0	0	0	41.319	
	$c=6.85437$						
P2 ₁ (4) <i>monoclinic</i> K ₂ O-type-III	$\alpha=\beta=\gamma=90$						-1273.1680
	$a=6.47342$	K1(2a)	0.92715	0.86935	0.79390	242.517	
	$b=7.57681$	K2(2a)	0.73534	0.49938	0.70714	45.797	
	$c=4.94451$	K3(2a)	0.76879	0.04564	0.33056		
	$\alpha=\gamma=90$	K4(2a)	0.55935	0.67889	0.21101		
	$\beta=90.08930$	O1(2a)	0.02152	0.21333	0.71134		
P2 ₁ /m (11) <i>monoclinic</i> K ₂ O-type-IV		O2(2a)	0.49721	0.82369	0.71755		-1273.0894
	$a=6.00231$	K1(2e)	0.05871	1/4	0.22623	229.655	
	$b=4.89708$	K2(2e)	0.21736	1/4	0.88991	50.516	
	$c=7.97209$	K3(2e)	0.55715	1/4	0.22215		
	$\alpha=\gamma=90$	K4(2e)	0.38838	1/4	0.55839		
	$\beta=101.46400$	O1(2e)	0.71892	1/4	0.89242		
Cmcm (63) <i>orthorhombic</i> K ₂ O-type-V		O2(2e)	0.88451	1/4	0.55502		-1273.1259
	$a=8.86822$	K1(8g)	0.33562	0.20350	1/4	226.512	
	$b=5.12198$	O1(4c)	0	0.21036	1/4	56.975	
	$c=4.98673$						
P2/c (15) <i>monoclinic</i> K ₂ O-type-VI	$\alpha=\beta=\gamma=90$						-1273.1243
	$a=5.09435$	K1(4e)	0	0.06809	1/4	227.919	
	$b=8.84211$	K2(4e)	0	0.73241	1/4	56.056	
	$c=5.49727$	O1(4e)	0	0.39788	1/4		
P2/c (15) <i>monoclinic</i> K ₂ O-type-VII	$\beta=113.01180$						-1273.1214
	$a=8.87576$	K1(8f)	0.83188	0.84966	0.75202	227.756	
	$b=5.17160$	O1(4e)	0	0.64326	1/4	56.037	
	$c=7.24678$						
Pmna (62) <i>orthorhombic</i> K ₂ O-type-VIII	$\alpha=\beta=\gamma=90$						-1273.1011
	$a=5.93377$	K1(4c)	0.89185	1/4	0.24671	227.828	
	$b=4.32641$	K2(4c)	0.86140	1/4	0.58217	48.153	
	$c=8.87462$	O1(4c)	0.86168	1/4	0.91300		
Pm (6) <i>monoclinic</i> K ₂ O-type-IX	$\alpha=\beta=\gamma=90$						-1273.0824
	$a=7.54569$	K1(2c)	0.79441	0.74728	0.31688	228.870	
	$b=6.09072$	K2(2c)	0.13174	0.75354	0.08841	47.372	
	$c=5.11811$	K3(2c)	0.46304	0.25094	0.55810		
	$\alpha=\gamma=90$	K4(1a)	0.79574	0	0.82128		
	$\beta=103.34560$	K5(1b)	0.13112	1/2	0.59146		
		O1(1a)	0.12558	0	0.58376		
		O2(1b)	0.46008	1/2	0.05854		
	O3(1b)	0.80457	1/2	0.81877			
	O4(1a)	0.46578	0	0.05693			

TABLE IX. Data for structure candidates for K₂O after local optimizations on the *ab initio* level (DFT-B3LYP).

Space group (no.) crystal system, type	Lattice constants a, b, c (Å); α, β, γ (°)	Atom (multip., Wyckoff lett.), rel. coord.				V_{\min} (Å ³) B (GPa)	E_{\min} (a.u.)
		atom	x	y	z		
<i>C2</i> (5) <i>monoclinic</i> K ₂ O-type-I	$a=19.78408$	K1(4c)	0.07822	0.92669	0.52962	398.442	-1274.9598
	$b=4.42676$	K2(4c)	0.08240	0.43873	0.06776	39.030	
	$c=4.55371$	K3(4c)	0.23285	0.92288	0.76198		
	$\alpha=\gamma=90$	O1(2a)	0	0.95014	0		
	$\beta=92.46470$	O2(4c)	0.16011	0.41961	0.58447		
<i>Immm</i> (71) <i>orthorhombic</i> K ₂ O-type-II	$a=4.11845$	K1(4j)	1/2	0	0.72688	131.171	-1274.9596
	$b=4.65374$	O1(2a)	0	0	0	39.043	
	$c=6.84385$						
	$\alpha=\beta=\gamma=90$						
<i>P2</i> ₁ (4) <i>monoclinic</i> K ₂ O-type-III	$a=6.46615$	K1(2a)	0.92715	0.86935	0.79390	241.702	-1274.9553
	$b=7.56831$	K2(2a)	0.73534	0.49938	0.70714	46.353	
	$c=4.93896$	K3(2a)	0.76879	0.04564	0.33056		
	$\alpha=\gamma=90$	K4(2a)	0.55935	0.67889	0.21101		
	$\beta=90.08930$	O1(2a)	0.02152	0.21333	0.71134		
		O2(2a)	0.49721	0.82369	0.71755		
<i>P2</i> ₁ / <i>m</i> (11) <i>monoclinic</i> K ₂ O-type-IV	$a=6.03706$	K1(2e)	0.05871	1/4	0.22623	233.674	-1274.8863
	$b=4.92550$	K2(2e)	0.21736	1/4	0.88991	43.844	
	$c=8.01837$	K3(2e)	0.55715	1/4	0.22215		
	$\alpha=\gamma=90$	K4(2e)	0.38838	1/4	0.55839		
	$\beta=101.46400$	O1(2e)	0.71892	1/4	0.89242		
		O2(2e)	0.88451	1/4	0.55502		
<i>Cmcm</i> (63) <i>orthorhombic</i> K ₂ O-type-V	$a=8.91616$	K1(8g)	0.33562	0.20350	1/4	230.205	-1274.9175
	$b=5.14967$	O1(4c)	0	0.21036	1/4	45.410	
	$c=5.01368$						
	$\alpha=\beta=\gamma=90$						
<i>P2</i> / <i>c</i> (15) <i>monoclinic</i> K ₂ O-type-VI	$a=5.12215$	K1(4e)	0	0.06809	1/4	231.670	-1274.9158
	$b=8.89037$	K2(4e)	0	0.73241	1/4	44.944	
	$c=5.52727$	O1(4e)	0	0.39788	1/4		
	$\alpha=\gamma=90$						
	$\beta=113.01180$						
<i>P2</i> / <i>c</i> (15) <i>monoclinic</i> K ₂ O-type-VII	$a=8.92560$	K1(8f)	0.83188	0.84966	0.75202	231.614	-1274.9131
	$b=5.20063$	O1(4e)	0	0.64326	1/4	44.879	
	$c=7.28747$						
	$\alpha=\gamma=90$						
	$\beta=136.78870$						
<i>Pmna</i> (62) <i>orthorhombic</i> K ₂ O-type-VIII	$a=5.97099$	K1(4c)	0.89185	1/4	0.24671	232.143	-1274.8962
	$b=4.35355$	K2(4c)	0.86140	1/4	0.58217	43.594	
	$c=8.93029$	O1(4c)	0.86168	1/4	0.91300		
	$\alpha=\beta=\gamma=90$						
<i>Pm</i> (6) <i>monoclinic</i> K ₂ O-type-IX	$a=7.59803$	K1(2c)	0.79441	0.74728	0.31688	233.666	-1274.8797
	$b=6.13299$	K2(2c)	0.13174	0.75354	0.08841	35.356	
	$c=5.15361$	K3(2c)	0.46304	0.25094	0.55810		
	$\alpha=\gamma=90$	K4(1a)	0.79574	0	0.82128		
	$\beta=103.34560$	K5(1b)	0.13112	1/2	0.59146		
		O1(1a)	0.12558	0	0.58376		
		O2(1b)	0.46008	1/2	0.05854		
		O3(1b)	0.80457	1/2	0.81877		
		O4(1a)	0.46578	0	0.05693		

TABLE X. Data for structure candidates for Rb₂O after local optimizations on the *ab initio* level (Hartree-Fock).

Space group (no.) crystal system, type	Lattice constants a, b, c (Å); α, β, γ (°)	Atom (multip., Wyckoff lett.), rel. coord.				V_{\min} (Å ³) B (GPa)	E_{\min} (a.u.)
		atom	x	y	z		
<i>C2/m</i> (12) <i>monoclinic</i> Rb ₂ O-type-I	$a=9.18299$	Rb1(4i)	0.66434	0	0.20908	142.085	-122.4264
	$b=4.68607$	O1(2c)	0	0	1/2	49.810	
	$c=3.33321$						
	$\alpha=\gamma=90$ $\beta=97.86680$						
<i>Imm2</i> (44) <i>orthorhombic</i> Rb ₂ O-type-II	$a=11.81993$	Rb1(4c)	0.14245	0	0.72457	412.222	-122.4271
	$b=3.33955$	Rb2(4c)	0.19055	0	0.40946	45.886	
	$c=10.44308$ $\alpha=\beta=\gamma=90$	Rb3(2b)	0	1/2	0.93926		
		Rb4(2b)	0	1/2	0.24968		
		O1(4c)	0.82998	0	0.09680		
O2(2b)	0	1/2	0.54004				
<i>Pmna</i> (62) <i>orthorhombic</i> Rb ₂ O-type-III	$a=6.27113$	Rb1(4c)	0.55300	1/4	0.77799	278.421	-122.4725
	$b=4.86654$	Rb2(4c)	0.18011	1/4	0.06723	52.084	
	$c=9.12296$ $\alpha=\beta=\gamma=90$	O1(4c)	0.19509	1/4	0.39585		
<i>Pmna</i> (62) <i>orthorhombic</i> Rb ₂ O-type-IV	$a=8.47683$	Rb1(4c)	0.44853	1/4	0.64504	283.748	-122.4427
	$b=3.38912$	Rb2(4c)	0.88626	1/4	0.39901	41.431	
	$c=9.87673$ $\alpha=\beta=\gamma=90$	O1(4c)	0.74461	1/4	0.12645		

TABLE XI. Data for structure candidates for Rb₂O after local optimizations on the *ab initio* level (DFT-B3LYP).

Space group (no.) crystal system, type	Lattice constants a, b, c (Å); α, β, γ (°)	Atom (multip., Wyckoff lett.), rel. coord.				V_{\min} (Å ³) B (GPa)	E_{\min} (a.u.)
		atom	x	y	z		
<i>C2/m</i> (12) <i>monoclinic</i> Rb ₂ O-type-I	$a=9.15454$	Rb1(4i)	0.66434	0	0.20908	140.769	-123.3439
	$b=4.67155$	O1(2c)	0	0	1/2	43.703	
	$c=3.32288$						
	$\alpha=\gamma=90$ $\beta=97.86680$						
<i>Imm2</i> (44) <i>orthorhombic</i> Rb ₂ O-type-II	$a=11.78731$	Rb1(4c)	0.14245	0	0.72457	408.818	-123.3450
	$b=3.33033$	Rb2(4c)	0.19055	0	0.40946	45.964	
	$c=10.41426$ $\alpha=\beta=\gamma=90$	Rb3(2b)	0	1/2	0.93926		
		Rb4(2b)	0	1/2	0.24968		
		O1(4c)	0.82998	0	0.09680		
O2(2b)	0	1/2	0.54004				
<i>Pmna</i> (62) <i>orthorhombic</i> Rb ₂ O-type-III	$a=6.26419$	Rb1(4c)	0.55300	1/4	0.77799	277.498	-123.3856
	$b=4.86116$	Rb2(4c)	0.18011	1/4	0.06723	44.052	
	$c=9.11287$ $\alpha=\beta=\gamma=90$	O1(4c)	0.19509	1/4	0.39585		
<i>Pmna</i> (62) <i>orthorhombic</i> Rb ₂ O-type-IV	$a=8.45303$	Rb1(4c)	0.44853	1/4	0.64504	281.365	-123.3584
	$b=3.37960$	Rb2(4c)	0.88626	1/4	0.39901	41.958	
	$c=9.84902$ $\alpha=\beta=\gamma=90$	O1(4c)	0.74461	1/4	0.12645		

TABLE XII. Data for structure candidates for Cs₂O after local optimizations on the *ab initio* level (Hartree-Fock).

Space group (no.) crystal system, type	Lattice constants a, b, c (Å); α, β, γ (°)	Atom (multip., Wyckoff lett.), rel. coord.				V_{\min} (Å ³) B (GPa)	E_{\min} (a.u.)
		atom	x	y	z		
<i>Pmna</i> (62) <i>orthorhombic</i> Cs ₂ O-type-I	$a=9.05524$	Cs1(4c)	0.18375	1/4	0.47463	382.481	-114.5676
	$b=3.91570$	Cs2(4c)	0.00126	1/4	0.80457	31.602	
	$c=10.78699$	O1(4c)	0.73888	1/4	0.35440		
	$\alpha=\beta=\gamma=90$						
<i>P2₁</i> (4) <i>monoclinic</i> Cs ₂ O-type-II	$a=5.98742$	Cs1(2a)	0.47801	0.21938	0.37836	351.875	-114.4812
	$b=6.15184$	Cs2(2a)	0.92848	0.99619	0.21204	34.581	
	$c=9.65125$	Cs3(2a)	0.97870	0.52435	0.41024		
	$\alpha=\gamma=90$	Cs4(2a)	0.64794	0.48089	0.01767		
	$\beta=98.17860$	O1(2a)	0.83443	0.94625	0.88265		
		O2(2a)	0.47156	0.72994	0.28989		

ori experimental knowledge of the system. However, this contradicts the premise of our approach, i.e., to identify the stable and metastable modifications of a chemical system without any prior information except the identity of the participating atoms. Of course, one can attempt to fit the parameters of the empirical potential to the *ab initio* calculations in the system, but this typically involves a large amount of effort. Finally, we have found that many of these potentials are not globally applicable. They strongly favor the structure(s) to which they have been fitted, and even successfully reproduce their properties. But at the same time, these potentials often weaken or even eliminate the minima representing important alternative modifications on the landscape of the chemical system.

Thus, in order to overcome the limitations of the simple potential as much as possible while still retaining its advantages, we repeat our global explorations for slightly varied values of the parameters r_s , ϵ_{ij} , and μ .⁵⁰ Our experience over the past decade has shown that the most important structure candidates usually are quite robust, i.e., they are found as local minima on many of the slightly modified energy landscapes. Furthermore, this also allows us to address the con-

cern that for many elements the effective ionic radius of an atom in a compound varies as function of the number of atoms in the first coordination sphere around the atom. As far as the identification of structure candidates is concerned, this systematic variation of the atom size has a similar effect as one would expect from employing a potential that explicitly contains such a size variation, such as the breathing potentials^{5,79-91} or the environment-dependent potential^{51,52} we have employed in the past. In the study presented here, we have found that the parameter variation by $\pm 10\%$ about the standard values for the system ($r_s=1.1$, $\epsilon_{ij}=0.4$, $\mu=0.1$) did not result in new relevant structure candidates. All candidate structures that were energetically favorable on the *ab initio* level occurred as local minima for many values of the parameters of the potential, including the standard values.

Regarding the pressure-homologue rule as applied to transition pressures, it appears to be obeyed by the alkali metal oxides for the transition pressures between the CaF₂-type and the first high-pressure modifications, in agreement with empirically based expectations from other chemical systems. But perhaps an even more noteworthy observation is the dramatic shrinkage of the stability range of the CaF₂-structure

TABLE XIII. Data for structure candidates for Cs₂O after local optimizations on the *ab initio* level (DFT-B3LYP).

Space group (no.) crystal system, type	Lattice constants a, b, c (Å); α, β, γ (°)	Atom (multip., Wyckoff lett.), rel. coord.				V_{\min} (Å ³) B (GPa)	E_{\min} (a.u.)
		atom	x	y	z		
<i>Pmna</i> (62) <i>orthorhombic</i> Cs ₂ O-type-I	$a=8.93372$	Cs1(4c)	0.18375	1/4	0.47463	367.287	-115.4801
	$b=3.86315$	Cs2(4c)	0.00126	1/4	0.80457	31.457	
	$c=10.64223$	O1(4c)	0.73888	1/4	0.35440		
	$\alpha=\beta=\gamma=90$						
<i>P2₁</i> (4) <i>monoclinic</i> Cs ₂ O-type-II	$a=5.98581$	Cs1(2a)	0.47801	0.21938	0.37836	351.592	-152.6416
	$b=6.15019$	Cs2(2a)	0.92848	0.99619	0.21204	34.085	
	$c=9.64866$	Cs3(2a)	0.97870	0.52435	0.41024		
	$\alpha=\gamma=90$	Cs4(2a)	0.64794	0.48089	0.01767		
	$\beta=98.17860$	O1(2a)	0.83443	0.94625	0.88265		
		O2(2a)	0.47156	0.72994	0.28989		

type from Li_2O to Rb_2O , and finally the complete elimination for Cs_2O . This decrease in the stability range takes place not only at the upper limit at positive high pressures, but also at the lower limit at negative ones—the transition pressure from the CaCl_2 -type modification to the CaF_2 -type continually grows with increasing cation size. Interestingly, starting at Li_2O as a highly metastable phase, the CdCl_2 -type becomes more and more stable, almost replacing CaF_2 in Rb_2O as the stable phase at standard pressures, and then becoming the structure of the stable phase for Cs_2O for a substantial pressure range including standard pressure. At the same time, the PbCl_2 -type modification becomes the first stable high-pressure phase, with a transition pressure of about 6 GPa.

The main competitors of the PbCl_2 -type in all systems from Li_2O to Rb_2O are the γ - US_2 - and the (hp)- BaF_2 -type, and we have found that for these four oxides the *ab initio* local optimization steers the PbCl_2 - and the (hp)- BaF_2 -type to essentially the same single minimum in the high-pressure range. Furthermore, for Li_2O , the γ - US_2 -type and the PbCl_2 -type modifications exhibit nearly the same enthalpy in the transition pressure range, while for Na_2O , K_2O , and Rb_2O , we first observe the PbCl_2 -/(hp)- BaF_2 -type followed by a transition to the γ - US_2 -type at higher pressures.

In other work on two classes of AB -systems,^{31,95} we have observed similar reductions of the stability range of phases in the interior of the phase diagram as function of cation size. The size of the stability ranges of both the so-called 5-5 (Ref. 50) and the rock salt modifications in the alkaline earth metal oxides,³¹ and the alkali metal halides⁹⁵ decrease with size of the cation for fixed choice of anion. Similarly, the range of stability of the intermediary phases, in particular the CaF_2 -type structure, in the alkali metal sulfides³⁰ decreases with increasing cation size (see Fig. 9). Thus, we suggest that an extension of the traditional pressure-homologue rule should hold: “The stability range of phases that lie in the interior of the one-dimensional pressure phase diagrams of a family of (ionic) compounds decreases with increasing size of the cations involved.”

V. SUMMARY AND OUTLOOK

We have globally explored the enthalpy landscapes of the alkali oxides for a wide range of pressures and found a large

number of kinetically stable structure candidates in these five systems. Local optimization of these candidates on the *ab initio* level resulted in the determination of the thermodynamically stable modifications in each system as function of pressure. At standard pressure, the computed phase agrees with the experimentally observed one for all five alkaline earth oxides. Of course, it would be very helpful if the predictions subsumed in the one-dimensional phase diagrams in Fig. 8 could be verified. Apart from the recent indications of a high-pressure phase of Li_2O , no results of experiments at high pressures or effective negative pressures on alkali oxides are known to us, although these compounds have been known for many decades. The reason for the lack of such studies (or definite answers from attempted investigations) might lie not so much in the difficulty to reach sufficiently high pressures. Instead, in most alkali oxides the possible decomposition into stable neighbor phases such as $M_2(\text{O}_2)$ or $M(\text{O}_2)$, or a high sensitivity to the influence of impurities, such as H_2O , at some stage of the experiment might play a role. Based on our experience with the analogous sulfides Li_2S ,⁹⁶ Na_2S ,⁹⁷ and K_2S ,⁹⁸ where all the transitions were reversible, we suspect that *in situ* measurements using diamond anvil cells would be needed to observe the high-pressure phases for the oxides exhibiting a $\text{CaF}_2 \rightarrow$ cotunnite-type [PbCl_2 , (hp)- BaF_2 , or γ - US_2] transition. In contrast, for Cs_2O a quenched high-pressure phase in the PbCl_2 -structure type might be kinetically stable and thus accessible with high-pressure quench methods.

ACKNOWLEDGMENTS

We would like to thank W. Klein, D. Fischer, and G. Stollhoff for many valuable discussions.

APPENDIX

Tables IV–XIII show the structural data for the most distinctive AB_2 -structure types for all alkali metal oxides $M_2\text{O}$ ($M=\text{Li}, \text{Na}, \text{K}, \text{Rb}, \text{Cs}$). Energies are given in hartree, bulk moduli B in gigapascal, and equilibrium volumes at zero pressure V_{min} in cubic angstroms. Because of the use of pseudopotentials and different basis sets, the values returned for the energies (per formula unit) are not directly comparable across calculational procedures.

¹L. Liu and W. A. Bassett, *Elements, Oxides and Silicates: High-Pressure Phases with Implications for the Earth's Interior* (Oxford University Press, London, 1986).

²*Ultrahigh-Pressure Mineralogy: Physics and Chemistry of the Earth's Deep Interior*, edited by R. J. Hemley, Reviews in Mineralogy, Vol. 37 (Mineralogical Society of America, Washington, DC, 1998).

³M. T. Yin and M. L. Cohen, Phys. Rev. Lett. **50**, 2006 (1983).

⁴M. L. Cohen, Int. J. Quantum Chem. **29**, 883 (1986).

⁵R. E. Cohen, Geophys. Res. Lett. **14**, 37 (1987).

⁶H. Cynn, D. G. Isaak, R. E. Cohen, M. F. Nicol, and O. L. Ander-

son, Am. Mineral. **75**, 439 (1990).

⁷M. L. Cohen, Z. Reut, L. J. Sham, P. B. Allen, N. W. Ashcroft, and V. Heine, Philos. Trans. R. Soc. London, Ser. A **334**, 501 (1991).

⁸R. E. Cohen, in *High Pressure Research in Mineral Physics: Application to Earth and Planetary Science*, edited by M. Manghiani and Y. Syono (AGU, Washington, DC, 1992), pp. 425–432.

⁹F. C. Marton and R. E. Cohen, Am. Mineral. **79**, 789 (1994).

¹⁰K. T. Thomson, R. M. Wentzcovitch, and M. S. T. Bukowinski, Am. Mineral. **79**, 789 (1994).

¹¹B. Winkler, Z. Kristallogr. **214**, 506 (1999).

- ¹²J. C. Schön, M. A. C. Wevers, and M. Jansen, *Solid State Commun.* **2**, 449 (2000).
- ¹³J. C. Schön, M. A. C. Wevers, and M. Jansen, *J. Mater. Chem.* **11**, 69 (2001).
- ¹⁴B. Winkler, C. J. Pickard, V. Milman, and G. Thimm, *Chem. Phys. Lett.* **337**, 36 (2001).
- ¹⁵R. T. Strong, C. J. Pickard, V. Milman, G. Thimm, and B. Winkler, *Phys. Rev. B* **70**, 045101 (2004).
- ¹⁶Ž. Čančarević, J. C. Schön, and M. Jansen, *Z. Anorg. Allg. Chem.* **631**, 1167 (2005).
- ¹⁷P. Kroll, T. Schröter, and M. Peters, *Angew. Chem., Int. Ed.* **44**, 4249 (2005).
- ¹⁸G. Bergerhoff, R. Hundt, R. Sievers, and I. D. Brown, *J. Chem. Inf. Comput. Sci.* **23**, 66 (1983).
- ¹⁹ICSD-Fiz-Karlsruhe, *Inorganic Crystal Structure Database*, <http://icsdweb.fiz-karlsruhe.de> (2005).
- ²⁰D. Fischer and M. Jansen, *Angew. Chem., Int. Ed.* **41**, 1755 (2002).
- ²¹D. Fischer and M. Jansen, *J. Am. Chem. Soc.* **124**, 3488 (2002).
- ²²D. Fischer and M. Jansen, *Z. Anorg. Allg. Chem.* **629**, 1934 (2003).
- ²³D. Fischer, Ž. Čančarević, J. C. Schön, and M. Jansen, *Z. Anorg. Allg. Chem.* **630**, 156 (2004).
- ²⁴W. Ostwald, *Z. Phys. Chem., Stoechiom. Verwandtschaftsftl.* **22**, 282 (1897).
- ²⁵J. C. Schön and M. Jansen, *Angew. Chem., Int. Ed. Engl.* **35**, 1286 (1996).
- ²⁶S. M. Woodley, P. D. Battle, J. D. Gale, and C. R. A. Catlow, *Phys. Chem. Chem. Phys.* **1**, 2535 (1999).
- ²⁷C. M. Draznieks, J. M. Newsam, A. M. Gorman, C. M. Freeman, and G. Ferey, *Angew. Chem., Int. Ed.* **39**, 2270 (2000).
- ²⁸J. C. Schön and M. Jansen, *Z. Kristallogr.* **216**, 307 (2001).
- ²⁹M. Jansen, *Angew. Chem., Int. Ed.* **41**, 3747 (2002).
- ³⁰J. C. Schön, Ž. Čančarević, and M. Jansen, *J. Chem. Phys.* **121**, 2289 (2004).
- ³¹J. C. Schön, *Z. Anorg. Allg. Chem.* **630**, 2354 (2004).
- ³²A. Neuhaus, *Chimia* **18**, 93 (1964).
- ³³E. Zintl, A. Harder, and B. Dauth, *Z. Elektrochem. Angew. Phys. Chem.* **40**, 588 (1934).
- ³⁴J. M. Bijvoet, A. Claassen, and A. Karssen, *Proc. K. Ned. Akad. Wet.* **29**, 1286 (1926).
- ³⁵P. Touzain, F. Brisse, and M. Caillet, *Can. J. Chem.* **48**, 3358 (1970).
- ³⁶A. Helms and W. Klemm, *Z. Anorg. Allg. Chem.* **242**, 33 (1939).
- ³⁷P. Touzain and M. Caillet, *Rev. Chim. Miner.* **8**, 277 (1971).
- ³⁸K. R. Tsai and P. M. Harris, *Phys. Rev.* **86**, 651 (1952).
- ³⁹K. R. Tsai, P. M. Harris, and E. Lassetre, *J. Phys. Chem.* **60**, 338 (1956).
- ⁴⁰S. Hull, T. Farley, W. Hayes, and M. Hutchings, *J. Nucl. Mater.* **160**, 125 (1988).
- ⁴¹K. Kunc, I. Loa, A. Grzechnik, and K. Syassen, *Phys. Status Solidi B* **242**, 1857 (2005).
- ⁴²R. Dovesi, C. Roetti, C. Freyria-Fava, M. Prencipe, and V. R. Saunders, *Chem. Phys.* **156**, 11 (1991).
- ⁴³R. Dovesi, C. Roetti, C. Freyria-Fava, E. Apra, V. R. Saunders, and N. M. Harrison, *Philos. Trans. R. Soc. London* **341**, 203 (1992).
- ⁴⁴L. Liu, V. E. Henrich, W. P. Ellis, and I. Shindo, *Phys. Rev. B* **54**, 2236 (1996).
- ⁴⁵A. Shukla, M. Dolg, P. Fulde, and H. Stoll, *J. Chem. Phys.* **108**, 8521 (1998).
- ⁴⁶J. G. Rodeja, M. Meyer, and M. Hayoun, *Modell. Simul. Mater. Sci. Eng.* **9**, 81 (2001).
- ⁴⁷E. A. Mikajlo, H. E. Dorsett, and M. J. Ford, *J. Chem. Phys.* **120**, 10799 (2004).
- ⁴⁸W. Jeitschko, *Acta Crystallogr., Sect. B: Struct. Crystallogr. Cryst. Chem.* **B24**, 930 (1968).
- ⁴⁹S. W. deLeeuw, J. W. Perram, and E. R. Smith, *Proc. R. Soc. London, Ser. A* **373**, 27 (1980).
- ⁵⁰J. C. Schön and M. Jansen, *Comput. Mater. Sci.* **4**, 43 (1995).
- ⁵¹H. Putz, J. C. Schön, and M. Jansen, *Comput. Mater. Sci.* **11**, 309 (1998).
- ⁵²H. Putz, J. C. Schön, and M. Jansen, *Z. Anorg. Allg. Chem.* **625**, 1624 (1999).
- ⁵³J. Emsley, *The Elements* (Clarendon Press, Oxford, 1992).
- ⁵⁴In order to investigate the possible structures in systems such as $M(O_2)$ or $M_2(O_2)$, it is necessary to introduce appropriate building units.^{28,102}
- ⁵⁵S. Kirkpatrick, C. D. Gelatt, Jr., and M. P. Vecchi, *Science* **220**, 671 (1983).
- ⁵⁶V. Czerny, *J. Optim. Theory Appl.* **45**, 41 (1985).
- ⁵⁷N. Metropolis, A. W. Rosenbluth, M. N. Rosenbluth, A. H. Teller, and E. Teller, *J. Chem. Phys.* **21**, 1087 (1953).
- ⁵⁸R. Hundt, J. C. Schön, A. Hannemann, and M. Jansen, *J. Appl. Crystallogr.* **32**, 413 (1999).
- ⁵⁹A. Hannemann, R. Hundt, J. C. Schön, and M. Jansen, *J. Appl. Crystallogr.* **31**, 922 (1998).
- ⁶⁰R. Hundt, J. C. Schön, and M. Jansen, *J. Appl. Crystallogr.* **39**, 6 (2006).
- ⁶¹R. Hundt, KPLLOT: A Program for Plotting and Investigation of Crystal Structures, University of Bonn, Germany, 1979.
- ⁶²Ž. Čančarević, J. C. Schön, and M. Jansen, *Mater. Sci. Forum* **453**, 71 (2004).
- ⁶³V. R. Saunders, R. Dovesi, C. Roetti, M. Causa, N. M. Harrison, R. Orlando, and C. M. Zicovich-Wilson, *CRYSTAL2003*, University of Torino, Torino, 2003.
- ⁶⁴A. D. Becke, *J. Chem. Phys.* **98**, 5648 (1993).
- ⁶⁵B3LYP in CRYSTAL is based on the “exact” form of the Vosko-Wilk-Nusair correlation potential (corresponds to a fit to the Ceperley-Adler data). In the original paper,¹⁰³ it is reported as a functional V , which is used to extract the “local” part of the LYP correlation potential. The Becke’s 3 parameter functional can be written as: $E_{xc} = (1-A)(E_x^{LDA} + B^* E_x^{BECKE}) + AE_x^{HF} + (1-C)E_c^{VWN} + CE_c^{LYP}$. Parameters A, B, and C are input data of HYBRYD and NONLOCAL keywords in CRYSTAL2003 and in this case have values 20, 0.9, and 0.81, respectively (for more details see *CRYSTAL2003 User’s Manual*⁶³).
- ⁶⁶F. D. Murnaghan, *Proc. Natl. Acad. Sci. U.S.A.* **30**, 244 (1944).
- ⁶⁷It follows from $H_i = H_j$ that the transition pressure p_c is given as the negative slope of the common tangent of $E_i(V)$ and $E_j(V)$.
- ⁶⁸Since our study required the comparison of energies for very different crystal configurations and structures, rather high accuracy was necessary. The self-consistent-field convergence criterion was taken to be changes in the total energy of $<10^{-8}$ Hartree.
- ⁶⁹The full heuristic algorithm⁶² contains the following steps: idealization (LOAD script), sorting (FILTER script), and preliminary ranking of the structure candidates found by global optimization, followed by a local optimization (HARTREE script).
- ⁷⁰In the present investigation, the following structure types belonged to the extended cotunnite family: $PbCl_2$ -, (hp)- BaF_2 -,

- γ -US₂-, Θ -Ni₂Si-, EuD₂-, NbGe₂-, and Co₂Si-type.
- ⁷¹M. Wevers, J. Schön, and M. Jansen, *J. Solid State Chem.* **136**, 223 (1998).
- ⁷²See EPAPS Document No. E-PRBMDO-73-010622 for additional tables and figures. Tables 1–10 show structural data, bulk moduli, and energies of the selected structure candidates for Li₂O, Na₂O, K₂O, Rb₂O, and Cs₂O. Figure 1 shows local optimization results using the HF method for 41 structure candidates in Li₂O. Figures 2–11 show results of local optimization using Hartree-Fock and DFT-B3LYP Hamiltonians for Li₂O, Na₂O, K₂O, Rb₂O, and Cs₂O. The document can be reached via a direct link in the online article's HTML reference section or via the EPAPS homepage (<http://www.aip.org/pubservs/epaps.html>).
- ⁷³According to the standard tolerances employed in the algorithm CMPZ,⁶⁰ PbCl₂, and (hp)-BaF₂ should be treated as two different structures, even though they are very closely related to each other (e.g., they have the same space group and Wyckoff positions of the atoms)
- ⁷⁴We have taken these effects as much as possible into account in our choice of basis sets and pseudopotentials for Cs.³⁰
- ⁷⁵R. A. Buckingham, *Proc. R. Soc. London, Ser. A* **168**, 264 (1938).
- ⁷⁶M. Born and K. Huang, *Dynamical Theory of Crystal Lattices* (Oxford University Press, London, 1954).
- ⁷⁷G. Dick and A. Overhauser, *Phys. Rev.* **112**, 90 (1958).
- ⁷⁸K. Fischer, H. Blitz, R. Haberkorn, and W. Weber, *Phys. Status Solidi B* **54**, 285 (1972).
- ⁷⁹U. Schröder, *Solid State Commun.* **4**, 347 (1966).
- ⁸⁰V. Nusslein and U. Schröder, *Phys. Status Solidi* **21**, 309 (1967).
- ⁸¹R. G. Gordon and Y. S. Kim, *J. Chem. Phys.* **56**, 3122 (1972).
- ⁸²A. J. Cohen and R. G. Gordon, *Phys. Rev. B* **14**, 4593 (1976).
- ⁸³C. Muhlhausen and R. G. Gordon, *Phys. Rev. B* **23**, 900 (1981).
- ⁸⁴L. L. Boyer, M. J. Mehl, J. L. Feldman, J. R. Hardy, J. W. Flocken, and C. Y. Fong, *Phys. Rev. Lett.* **54**, 1940 (1985).
- ⁸⁵M. J. Mehl, R. J. Hemley, and L. L. Boyer, *Phys. Rev. B* **33**, 8685 (1986).
- ⁸⁶G. H. Wolf and M. S. T. Bukowinski, *Phys. Chem. Miner.* **15**, 209 (1988).
- ⁸⁷M. D. Jackson and R. G. Gordon, *Phys. Chem. Miner.* **16**, 212 (1988).
- ⁸⁸O. V. Ivanov and E. G. Maksimov, *Phys. Rev. Lett.* **69**, 108 (1992).
- ⁸⁹D. J. Lacks and R. G. Gordon, *Phys. Rev. B* **48**, 2889 (1993).
- ⁹⁰H. T. Stokes, L. L. Boyer, and M. J. Mehl, *Phys. Rev. B* **54**, 7729 (1996).
- ⁹¹L. L. Boyer, H. T. Stokes, and M. J. Mehl, *Ferroelectrics* **194**, 1173 (1997).
- ⁹²R. E. Cohen, in *MSA Reviews in Mineralogy; Silica: Physical Behavior, Geochemistry, and Materials Applications*, edited by P. Heaney, C. Prewitt, and G. Gibbs (Mineralogical Society of America, Washington, DC, 1994), Vol. 29, pp. 369–402.
- ⁹³L. Stixrude, R. E. Cohen, and R. J. Hemley, in *MSA Reviews in Mineralogy; Ultrahigh-Pressure Mineralogy*, edited by R. Hemley (Mineralogical Society of America, Washington, DC, 1998), Vol. 37, pp. 639–671.
- ⁹⁴B. B. Karki, L. Stixrude, and R. M. Wentzcovitch, *Rev. Geophys.* **39**, 507 (2001).
- ⁹⁵Ž. Čančarević, J. C. Schön, and M. Jansen (unpublished).
- ⁹⁶A. Grzechnik, A. Vegas, K. Syassen, I. Loa, M. Hanfland, and M. Jansen, *J. Solid State Chem.* **154**, 603 (2000).
- ⁹⁷A. Vegas, A. Grzechnik, K. Syassen, I. Loa, M. Hanfland, and M. Jansen, *Acta Crystallogr., Sect. B: Struct. Sci.* **57**, 151 (2001).
- ⁹⁸A. Vegas, A. Grzechnik, M. Hanfland, C. Mühle, and M. Jansen, *Solid State Sci.* **4**, 1077 (2002).
- ⁹⁹G. F. Carter, J. L. Margrave, and D. H. Templeton, *Acta Crystallogr.* **5**, 851 (1952).
- ¹⁰⁰D. Taylor, *Br. Ceram. Trans. J.* **83**, 32 (1984).
- ¹⁰¹T. W. D. Farley, W. Hayes, S. Hull, M. T. Hutchings, and M. Vrtis, *J. Phys.: Condens. Matter* **3**, 4761 (1991).
- ¹⁰²J. C. Schön and M. Jansen, *Acta Crystallogr., Sect. A: Found. Crystallogr. (Suppl.)* **55**, Abstract M13.DD.002 (1999).
- ¹⁰³S. H. Vosko, L. Wilk, and M. Nusair, *Can. J. Phys.* **58**, 1200 (1980).